

## Probing magneto-optic trap dynamics through weak excitation of a coupled narrow-linewidth transition

T. Loftus, J. R. Bochinski, and T. W. Mossberg

*Oregon Center for Optics and Department of Physics, University of Oregon, Eugene, Oregon 97403*

(Received 23 December 1999; published 2 May 2000)

Alkaline-earth-like atoms possess singlet and triplet manifolds coupled through the ground state. The weak and hence narrow linewidth intercombination transition can provide a powerful probe of singlet-singlet magneto-optic trap (MOT) dynamics. We demonstrate *in situ* probing of an ytterbium MOT and discuss how cloud position, size, and temperature can be determined.

PACS number(s): 32.80.Pj, 42.05.Vk, 95.30.Ky, 32.10.-f

Ytterbium (Yb,  $Z=70$ ) and other alkaline-earth-like atoms possess coupled two-level-like transitions (see Fig. 1) whose widely different natural widths [1,2] support multiple magneto-optic trapping opportunities. Specifically, the strong and nearly closed [3]  $^1S_0$ - $^1P_1$  transitions are well suited, due to their large scattering rates, to cooling atomic beams [2,4-6,9,10] and loading magneto-optic traps (MOTs) from thermal or slowed sources [4-6,9,10]. In contrast, and due to their narrow linewidths, the spin-forbidden  $^1S_0$ - $^3P_1$  transitions support MOTs with ultralow limiting temperatures and potentially high spatial densities [5,7], and are useful for high-resolution spectroscopic studies [8-10]. Employing these two types of transitions in complementary cooling, trapping, and spectroscopic roles may ultimately provide new routes to quantum degeneracy [5,7] and high-precision optical frequency standards [1,8-10]. A staged cooling experiment using first the  $^1S_0$ - $^1P_1$  and then the  $^1S_0$ - $^3P_1$  transitions in strontium (Sr) has already led to record phase-space densities in a MOT [5]. Additionally, optical spectroscopy of the  $^1S_0$ - $^3P_1$  magnesium (Mg) [9] (calcium (Ca) [10]) transition in  $^1S_0$ - $^1P_1$  MOTs has produced fractional frequency stabilities exceeding (approaching) that which can be obtained with atomic-beam experiments using the same species.

In this Rapid Communication, we present observations, in a steady-state 398.8-nm  $(6s^2)^1S_0$ - $(6s6p)^1P_1$   $^{174}\text{Yb}$  MOT, of probe fluorescence spectra induced by excitation of the  $^{174}\text{Yb}(6s^2)^1S_0$ - $(6s6p)^3P_1$  555.6-nm transition. We find that the Zeeman structure of the  $^3P_1$  excited state is completely resolved and that peak widths and splittings provide diagnostic information about the atomic cloud size, location relative to the trap magnetic field zero [11], and potentially, the atomic velocity distribution [10]. Use of an intercombination transition to perform *in situ* temperature measurements may provide an alternative approach to trap-destructive time-of-flight techniques [10,12].

Since a detailed description of the apparatus has been given previously [4], we only review the relevant features of the trapping experiment here. Approximately  $10^6$   $^{174}\text{Yb}$  atoms, loaded with a  $\sigma^-$  Zeeman slower, are held in a  $^1S_0$ - $^1P_1$  Yb MOT. For the power levels used in this experiment, the trap lifetime  $\tau$  is limited primarily by radiative branching from the  $^1P_1$  state to  $\tau \sim 400$  msec [4]. Trap axial

magnetic field gradients  $B'_z$  range in magnitude from 35 to 160 G/cm. Vacuum levels during the experiment are  $< 10^{-8}$  Torr.

Fluorescence from the MOT is imaged onto a photomultiplier tube (PMT) whose output is sampled by a digital oscilloscope with an overall system response time of 500  $\mu\text{sec}$ . A 555-nm filter (bandpass width  $\Delta\lambda \sim 10$  nm) placed in front of the PMT allows selective detection of the 555.6-nm probe-induced fluorescence from the trap. The 555.6-nm probe beam is produced by a ring dye laser, RDL (long-term linewidth  $< 2$  MHz) whose output is attenuated to  $\sim 200$   $\mu\text{W}$  and combined with a trapping beam traveling normal to the axis of the anti-Helmholtz magnetic field coils. The collimated probe beam has a  $1/e^2$  intensity diameter of 1.5 cm, is single-passed through the atom cloud, and has approximately the same circular polarization as the trapping beam that copropagates with it. Saturated absorption in an external Yb gas cell provides a frequency marker for the  $^{174}\text{Yb}$   $^1S_0$ - $^3P_1$  resonance.

A time-of-flight estimate of the trap temperature was made with the probe beam by monitoring probe fluorescence as a function of time after the 398.8-nm trapping beams were extinguished. For this measurement, a 555.6-nm standing-wave probe beam with  $\sim 3$   $\mu\text{W}$  per traveling-wave component was employed. We find that the atom cloud temperature is  $\sim 2$  mK, or about three times the Doppler-limited temperature,  $T_D = 670$   $\mu\text{K}$  of the  $^1S_0$ - $^1P_1$  line. We point out that this value is 30 times smaller than the measured upper limit reported by Honda *et al.* [6].

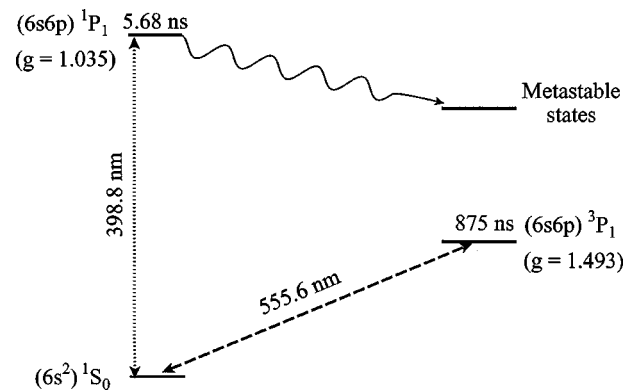


FIG. 1. A partial energy-level diagram for  $^{174}\text{Yb}$ . Lande  $g$  factors for the  $^1P_1$  and  $^3P_1$  excited states are given in parentheses.

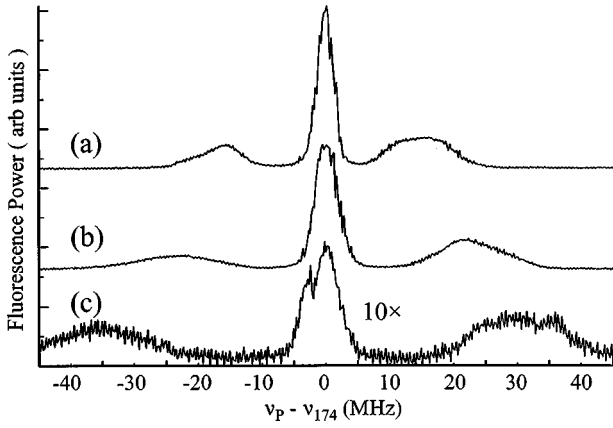


FIG. 2. Probe-induced 555.6-nm fluorescence versus probe frequency for different intensity imbalances in the trapping beams.  $\nu_p$  ( $\nu_{174}$ ) is the probe beam ( $^{174}\text{Yb } ^1S_0\text{-}^3P_1$  resonance) frequency. In (a) an intensity imbalance of  $\sim 30\%$ , arising purely from absorptive retroreflection optics, is employed. In (b) and (c) neutral density filters reduce the intensity of one of the retroreflected trapping beams by a factor of 2 and 4, respectively.

In the following, the summed power in the three 398.8-nm trapping beams (retroreflected to form standing waves) is 14 mW. The trapping beams are tuned  $-30$  MHz below the  $^{174}\text{Yb } ^1S_0\text{-}^1P_1$  resonance.

In Fig. 2, we plot probe-generated 555.6-nm fluorescence as a function of the probe frequency  $\nu_p$ , in the vicinity of the  $^{174}\text{Yb } ^1S_0\text{-}^3P_1$  transition frequency  $\nu_{174}$ . A three-peak spectrum is observed. In trace (a), the two traveling-wave components of each standing-wave trapping beam are balanced with  $\sim 30\%$  intensity difference (the best balance achievable with our retroreflection geometry). In traces (b) and (c), the retroreflected component of the trapping beam parallel to the anti-Helmholtz coil axis,  $z$ , is attenuated by a factor of 2 and 4, respectively.  $B'_z = 60$  G/cm throughout. As the power imbalance of the standing-wave trapping field components increases, the splitting of the three-peaked structure increases. In addition, the widths of all three peaks increase, with the central peak width experiencing the largest fractional gain.

We identify the three peaks in the probe spectrum with the three magnetically split Zeeman components of the  $^1S_0\text{-}^3P_1$  transition. In Fig. 3(a), we schematically plot the MOT magnetic-field magnitude  $|\vec{B}|$  versus position along a line passing through the zero-field point of the MOT. Below this we depict a cloud of cold atoms with diameter  $\Delta S$  and displacement  $S$  from the field null. In Fig. 3(b), we depict the  $^1S_0\text{-}^3P_1$  transition structure for atoms within the cloud. The Zeeman levels are split by  $S\mu_g B' + \epsilon$ , where  $-\Delta S\mu_g B'/2 < \epsilon < \Delta S\mu_g B'/2$  and  $B'$  is the magnetic-field gradient along the line considered. The narrowness of the  $^1S_0\text{-}^3P_1$  transition and the smallness of  $\Delta S$  relative to  $S$  allow for the appearance of a well-resolved spectral triplet. The side peaks are broadened by the magnetic-field variation across the atom cloud, while all three peaks are broadened by trap Doppler effects, the laser linewidth, and the effective natural width of the  $^1S_0\text{-}^3P_1$  transition as modified by the 398.8-nm trapping beams (Rabi broadening). The relative heights of the three peaks are determined by the local magnetic-field

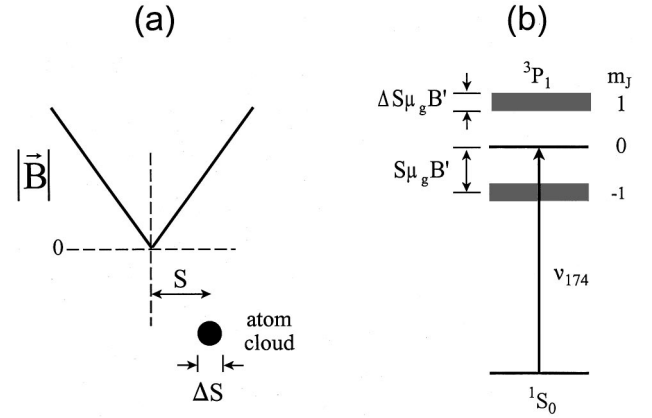


FIG. 3. (a) Schematic plot of the MOT magnetic-field magnitude versus position along a line passing through the magnetic-field zero point. The atomic cloud is displaced from the field zero by  $S$  and has a width  $\Delta S$ . (b)  $^1S_0\text{-}^3P_1$  transition structure for atoms in the cloud.  $\mu_g = g\mu_B m_j/h$ , where  $g$  is the Landé  $g$  factor for the  $^3P_1$  excited state,  $\mu_B$  is the Bohr magneton,  $m_j$  is the magnetic quantum number, and  $h$  is Planck's constant.  $\nu_{174}$  is the  $^1S_0(m_j=0)\text{-}^3P_1(m_j=0)$  transition frequency.

geometry and the polarization of the probe beam. Interestingly, we found, in a separate series of measurements, that by changing the polarization of the probe beam we could modify the relative heights of the three features. The  $^1S_0\text{-}^1P_1$  trapping transition is split similarly, but the transition's 28-MHz natural width and a smaller Landé  $g$  factor [1] prevent the observation of the splitting under typical trap conditions.

The increased splitting observed in Fig. 2 indicates that increased power imbalance between the traveling-wave components of the relevant trapping field moves the atom into regions of higher magnetic field. Increased field may result from increased radial displacement, rotation toward a trap axis with a higher field gradient, or a combination. Current data do not allow for precise differentiation between these two mechanisms. However, previous studies have shown that power imbalance between components of standing-wave trapping beams promotes displacement along the axis of the imbalanced trapping beam [13].

In Fig. 4, we plot the 555.6-nm probe-induced fluorescence from a  $^{174}\text{Yb}$  MOT for different values of  $B'_z$ . From top to bottom,  $B'_z$  is 45, 100, and 140 G/cm, respectively. The peak splitting,  $\propto SB'_z$ , depends weakly on the gradient, implying that the atom cloud displacement from the magnetic field null,  $S$ , is inversely proportional to  $B'_z$ . Since the side peaks are significantly broader than the central peak, we conclude that broadening derived from magnetic-field inhomogeneity,  $\propto \Delta SB'_z$ , contributes significantly to their width. This fact, combined with the observation that the side peak widths are largely independent of  $B'_z$  allows us to conclude that the atomic cloud size scales inversely with  $B'_z$ . Note that these scaling relationships are in qualitative agreement with those expected from simple physical models of two-level atoms in a MOT [14]. Probe spectra as studied here provide a unique means for observational confirmation of these fundamental trap properties.

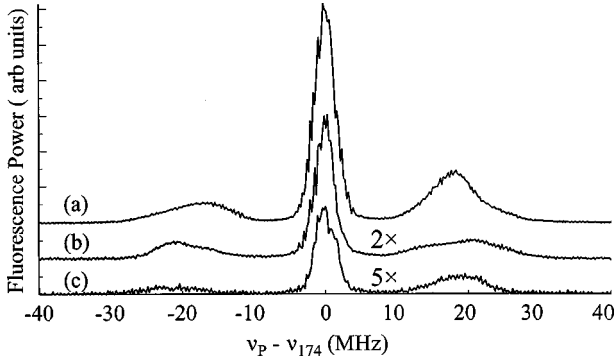


FIG. 4. Probe-induced 555.6-nm fluorescence versus probe frequency for different axial anti-Helmholtz magnetic-field gradients.  $\nu_p$  ( $\nu_{174}$ ) is the probe beam ( $^{174}\text{Yb } ^1S_0\text{-}^3P_1$  resonance) frequency.  $B'_z$  is (a) 45 G/cm, (b) 100 G/cm, and (c) 140 G/cm.

We have determined the total area under a family of traces like those of Fig. 4. To the extent that these areas scale with the number of atoms in the trap, one obtains a measure of trap population versus field gradient [see Fig. 5(a)]. For these measurements, the 398.8-nm trapping beams are tuned  $-30$  MHz below the  $^{174}\text{Yb } ^1S_0\text{-}^1P_1$  resonance, a value found to optimize the trap population  $N_T$  at  $B'_z = 45$  G/cm. Under these conditions,  $N_T$  is seen to decrease for higher or lower gradients, a result that is qualitatively similar to fixed detuning measurements of  $N_T$  versus magnetic-field gradient for alkali-metal MOTs [14].

In Figs. 5(b) and 5(c), respectively, we plot the cloud radius and displacement from the field null as a function of the axial magnetic field gradient. Plotted displacements  $S$  and radii  $\Delta S/2$  are normalized by the observed maximum at  $B'_z = 35$  G/cm and are calculated from measured peak splittings and widths according to

$$S = \frac{\Delta_s h}{|\nabla \vec{B}| g \mu_B m_J} \quad (1)$$

and

$$\frac{\Delta S}{2} = \frac{\Delta_w h}{|\nabla \vec{B}| g \mu_B m_J}, \quad (2)$$

where  $\Delta_s$  ( $\Delta_w$ ) is the observed peak splitting (the difference between the full width at half maximum widths of the central and side peaks),  $g \sim 1.5$  [1] is the Landé  $g$  factor for the  $^3P_1$  excited state,  $\mu_B$  is the Bohr magneton,  $m_J = \pm 1$  is the magnetic quantum number of the relevant peak, and  $h$  is Planck's constant. In choosing this definition for  $\Delta_w$ , we assume that broadening mechanisms due to trap Doppler effects, laser linewidth, and Rabi broadening of the  $^1S_0\text{-}^3P_1$  transition are given by the width of the central peak and ignore subtleties of deconvolution. As the gradient increases, we observe a trend toward smaller displacements and cloud radii [13,14]. Results in Figs. 5(b) and 5(c) are qualitative and assume primarily radial rather than angular repositioning as  $B'_z$  changes. Finally we note that the  $\sim 3$ -MHz center peak

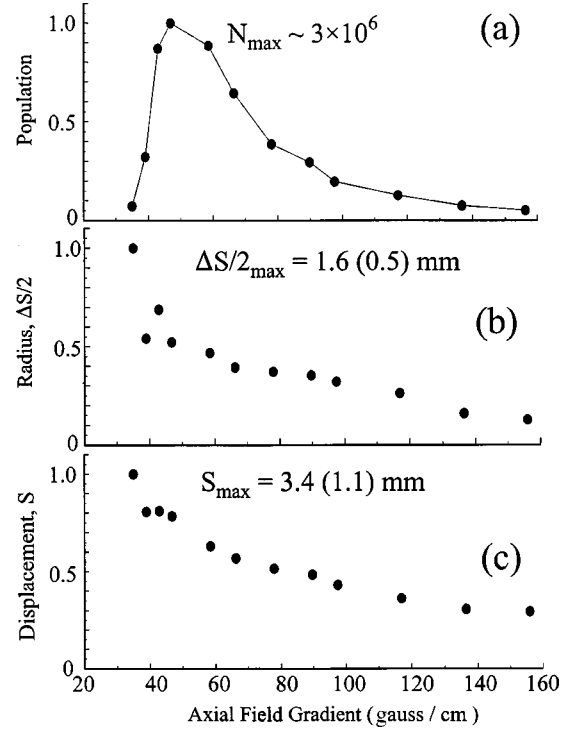


FIG. 5. Relative (a) trap population, (b) cloud radius  $\Delta S/2$ , and (c) cloud spatial displacement  $S$  all as a function of axial magnetic-field gradient. All traces are normalized by the observed maxima,  $N_{\max}$ ,  $\Delta S/2_{\max}$ , and  $S_{\max}$ .  $N_{\max}$  was determined from measurements of the 398.8-nm trap fluorescence. Uncertainties in  $\Delta S/2_{\max}$ , and  $S_{\max}$  are due to the cylindrical symmetry of the magnetic field.

width [see Figs. 2(a) and 4], which arises from the combined effects of laser linewidth, and Doppler and Rabi broadening of the  $^1S_0\text{-}^3P_1$  transition set an upper limit of 10 mK on the atom cloud temperature. Higher temperatures would be evident through Doppler mediated increased central peak width. Such higher temperatures are suggested in Figs. 2(b) and 2(c), where the power imbalance of one of the trapping beams is increased.

In conclusion, we have demonstrated that narrow line-width transitions coupled to a trapping transition can provide detailed, *in situ*, and nondestructive diagnostics of trap properties and dynamics. We specifically demonstrate that fluorescence-detected probe excitation spectra provide information indicative of the atom-cloud size, population, and spatial displacement. We point out that measurements of the cloud location relative to the magnetic field null are relevant to determining the trap spring constant, an important quantity whose dynamic properties have not been measured for systems that do not support polarization gradient cooling. Along with radiation trapping effects, the spring constant will ultimately determine how much MOTs using the intrinsically simple  $^1S_0\text{-}^1P_1$  transitions can be compressed to high densities. Additionally, the width of the central spectral feature observed here promises to provide real-time information on the trap temperature, especially when combined with information about the effective Rabi frequency of the trapping beams or when measured while the trapping beams are briefly switched off. Future work will investigate this possibility.

We gratefully acknowledge financial support from the National Science Foundation under Grant No. PHY-9870223.

- [1] J. L. Hall, M. Zhu, and P. Buch, *J. Opt. Soc. Am. B* **6**, 2194 (1989); R. Drozdowski, M. Ignaciuk, J. Kwela, and J. Heldt, *Z. Phys. D: At., Mol. Clusters* **41**, 125 (1997); A. Godone and C. Novero, *Phys. Rev. A* **45**, 1717 (1992); W. C. Martin, R. Zalubas, and L. Hagan, in *Atomic Energy Levels—The Rare-Earth Elements* (U.S. GPO, Washington, DC, 1978); C. J. Bowers, D. Budker, E. D. Commins, D. DeMille, S. J. Freedman, A.-T. Nguyen, S.-Q. Shang, and M. Zolotarev, *Phys. Rev. A* **53**, 3103 (1996); J. Migdalek and W. E. Baylis, *J. Phys. B* **24**, L99 (1991); S. G. Porsev, Y. G. Rakhlina, and M. G. Kozlov, *Phys. Rev. A* **60**, 2781 (1999).
- [2] N. Beverini, F. Giammanco, E. Maccioni, F. Strumia, and G. Vissani, *J. Opt. Soc. Am. B* **6**, 2188 (1989); A. Witte, Th. Kisters, R. Riehle, and J. Helmcke, *ibid.* **9**, 1030 (1992); M. Watanabe, R. Ohmukai, U. Tanaka, K. Hayasaka, H. Imajo, and S. Urabe, *ibid.* **13**, 2377 (1996); R. Ohmukai, H. Imajo, K. Hayasaka, U. Tanaka, M. Watanabe, and S. Urabe, *Appl. Phys. B: Photophys. Laser Chem.* **64**, 547 (1997); N. Beverini, S. De Pascalis, E. Maccioni, D. Pereira, F. Strumia, G. Vissani, Y. Z. Wang, and C. Novero, *Opt. Lett.* **14**, 350 (1989).
- [3] The Mg  $^1S_0$ - $^1P_1$  transition is radiatively closed. See Ref. [9].
- [4] T. Loftus, J. R. Bochinski, R. Shivitz, and T. W. Mossberg, *Phys. Rev. A* **61**, 051401(R) (2000).
- [5] H. Katori, T. Ido, Y. Isoya, and M. Kuwata-Gonokami, *Phys. Rev. Lett.* **82**, 1116 (1999); T. Kuwamoto, K. Honda, Y. Takahashi, and T. Yabuzaki, *Phys. Rev. A* **60**, R745 (1999).
- [6] T. Kurosu and F. Shimizu, *Jpn. J. Appl. Phys., Part 2* **29**, L2127 (1990); T. Kurosu and F. Shimizu, *Jpn. J. Appl. Phys., Part 1* **31**, 908 (1992); F. Shimizu, *Hyperfine Interact.* **74**, 259 (1992); K. Honda, Y. Takahashi, T. Kuwamoto, M. Fujimoto, K. Toyoda, K. Ishikawa, and T. Yabuzaki, *Phys. Rev. A* **59**, R934 (1999).
- [7] P. D. Lett, W. D. Phillips, S. L. Rolston, C. E. Tanner, R. N. Watts, and C. I. Westbrook, *J. Opt. Soc. Am. B* **6**, 2084 (1989); D. J. Wineland and W. M. Itano, *Phys. Rev. A* **20**, 1521 (1979).
- [8] T. Kurosu, M. Morinaga, and F. Shimizu, *Jpn. J. Appl. Phys., Part 2* **31**, L273 (1992).
- [9] W. Ertmer, *Phys. Scr.* **T40**, 23 (1992); K. Sengstock, U. Sterr, G. Hennig, D. Bettermann, J. H. Muller, and W. Ertmer, *Opt. Commun.* **103**, 73 (1993); K. Sengstock, U. Sterr, J. H. Muller, V. Rieger, D. Bettermann, and W. Ertmer, *Appl. Phys. B: Photophys. Laser Chem.* **59**, 99 (1994); D. Bettermann, H. Hinderthur, J. H. Muller, J. L. Peng, V. Rieger, F. Ruschewitz, K. Sengstock, T. Sterr, and W. Ertmer, in *1996 Conference on Precision Electromagnetic Measurements*, Braunschweig, Germany, 1996, edited by A. Braun (IEEE, New York, 1996).
- [10] T. Kisters, K. Zeiske, F. Riehle, and J. Helmcke, *Appl. Phys. B: Photophys. Laser Chem.* **59**, 89 (1994); F. Riehle, I. Schnatz, A. Celikov, Th. Kisters, K. Zeiske, G. Zinner, and J. Helmcke, in *1996 Conference on Precision Electromagnetic Measurements*, Boulder, CO, 1994, edited by E. DeWeese and G. Bennett (IEEE, New York, 1994); C. W. Oates, M. Stephens, and L. W. Hollberg, in *1997 Digest of the IEEE/LEOS Summer Topical Meetings*, Orlando, FL, 1997 (IEEE, New York, 1997).
- [11] A pulsed experiment with cold  $^6\text{Li}$  released from a MOT recently resolved Raman transitions between hyperfine ground states and used the observed spectra to determine the cloud size and location. See T. A. Savard, S. R. Granade, K. M. O'Hara, M. E. Gehm, and J. E. Thomas, *Phys. Rev. A* **60**, 4788 (1999).
- [12] E. L. Raab, M. Prentiss, A. Cable, S. Chu, and D. E. Pritchard, *Phys. Rev. Lett.* **59**, 2631 (1987); P. D. Lett, R. N. Watts, C. I. Westbrook, W. D. Phillips, P. L. Gould, and H. J. Metcalf, *ibid.* **61**, 169 (1988).
- [13] A. M. Steane, M. Chowdhury, and C. J. Foot, *J. Opt. Soc. Am. B* **9**, 2142 (1992); C. D. Wallace, T. P. Dinneen, K. Y. N. Tan, A. Kumarakrishnan, P. L. Gould, and J. Javanainen, *ibid.* **11**, 703 (1994); C. G. Townsend, N. H. Edwards, C. J. Cooper, K. P. Zetie, C. J. Foot, A. M. Steane, P. Szriftgiser, H. Perrin, and J. Dalibard, *Phys. Rev. A* **52**, 1423 (1995).
- [14] K. Lindquist, M. Stephens, and C. Wieman, *Phys. Rev. A* **46**, 4082 (1992); A. Hope, D. Haubrich, G. Muller, W. G. Kaenders, and D. Meschede, *Europhys. Lett.* **22**, 669 (1993); W. Petrich, M. A. Anderson, J. R. Ensher, and E. A. Cornell, *J. Opt. Soc. Am. B* **11**, 1332 (1994).